XXXVI Ibero-Latin American
Congress on Computational
Methods in Engineering
CILAMCE
Rio de Janeiro, 22-25 Nov 2015

ON A DEPTH-AVERAGED NUMERICAL SIMULATION OF FLOW PHENOMENA IN SEDIMENTARY BASINS

Ney Augusto Dumont
Elvis Yuri Mamani
Carlos Andrés Aguilar
Hélvio F. C. Peixoto
Civil Engineering Department, PUC-Rio
Rua Marquês de São Vicente, 225, Gávea, 22451-900, Rio de Janeiro, Brazil

Alexandre Antonio de Oliveira Lopes
Stefane Lopes
Petrosoft Design
Av. Abelardo Bueno 1111 sala 357 Bloco Office 2, Rio de Janeiro, Brazil

Abstract. *The ultimate goal of the present developments is the depth-averaged simulation of three-dimensional transport phenomena in sedimentary basins. The continuity and momentum equations that govern the problem are by nature highly non-linear, domain-driven and time-dependent. However, it has become possible to reduce the depth-averaged equations to a stream function-vorticity model plus a complementary equation. A variationally hybrid boundary element formulation (HBEM) is used for the iterative solution of a problem in an arbitrarily shaped, irregular domain embedded in a regular finite-difference (FD) grid. In each iteration, the non-linear terms are taken into account from the previous results in the frame of a FD scheme, as an arbitrary particular solution for which the boundary conditions are of no relevancy. This estimate solution is then added to the homogeneous part of the differential equations, which have been numerically discretized in terms of the HBEM. Improved HBEM results are obtained after considering the boundary conditions of the problem as a whole. Uncontrollable round-off errors may occur if the FD particular solution related to the domain, non-linear terms is too far apart from the sought solution. A relaxation factor may be required to guarantee stability of the iterative process and convergence of results. Besides the formulation, the paper also presents a few numerical examples to validate the proposed model as well as to assess its performance in terms of convergence of results.*

Keywords: *Hybrid boundary elements, Navier Stokes equations, non-linear equations, irregular domains, embedded formulation.*

1 INTRODUCTION

The search for an efficient algorithm to deal with irregular domains can be traced back to several decades ago (Buzbee *et al.*, 1971). Techniques that embed a boundary integral mesh in a regular finite-difference grid have also already been explored in the literature (Elghaoui & Pasquetti, 1999; Le *et al.*, 2008), as well as techniques that make use of multiple finite-difference grids (Ghia *et al.*, 1982), to mention but a few references. Different techniques, such as using multidomains (Ramšak *et al.*, 2005) and various possibilities of linearization of the inherently non-linear equations (Sheu & Lin, 2004) also might be explored.

Since the time scale to be considered in the present developments is very large (thousands or millions of years) and the physical domain of interest is in general several hundred kilometers across, the sediment flow is predominantly horizontal and a simplification of the governing 3D Navier-Stokes equations seems to be justifiable, as elaborated by Tetzlaff & Harbaugh (1989). It consists in expressing the movement of the sediment particles in terms of a depth-averaged horizontal flow for an assumed velocity profile across the vertical direction of the sediment layer (Dumont, 2014), whose thickness and composition will vary with time and space.

In the following, the basic equations are laid down and some simplifications are shown. Although this is a development of a short paper recently published (Dumont *et al.*, 2015), several details still had to be omitted owing to space restriction. The generalization of the problem for a transient analysis and considering deposition and erosion, as proposed in the above paragraph, is a work in progress.

2 BASIC PROBLEM FORMULATION

2.1 Continuity equation

We are initially looking for the mathematical description of flow for an isotropic Newtonian fluid in terms of the spatial Cartesian coordinates (x, y, z), where z is vertical and points upwards starting from some reference coordinate, and the time t. The relevant quantities are the fluid density ρ, which is considered constant, and the flow velocity vector $q_i \equiv \langle u \quad v \quad w \rangle \equiv \langle \dot{x} \quad \dot{y} \quad \dot{z} \rangle$ of a particle moving from one point (x, y, z) with time. The flow continuity equation is simply

$$q_{i,i} = 0 \tag{1}$$

2.2 Momentum equation

The Navier-Stokes equation for an isotropic fluid flow is

$$\dot{q}_i + q_j q_{i,j} = \frac{1}{\rho}(-p_{,i} + \mu q_{i,jj}) + g_i \tag{2}$$

where, further to the definitions given for the continuity equation, μ is the fluid viscosity, taken as constant, $p \equiv p(x, y, z)$ is the hydrostatic pressure, and g_i is the acceleration of gravity, which acts only in the z direction.

Equation (2) is a particular case of the more general equation

$$\rho\left(\dot{q}_i + q_j q_{i,j}\right) = -p_{,i} + \left(\mu U_{ij}\right)_{,j} + \rho\left(g_i + \Omega_{ij} q_j\right) \tag{3}$$

where $U_{ij} = q_{i,j} + q_{j,i} - \frac{2}{3}\delta_{ij} q_{k,k}$ is the Navier-Stokes tensor and Ω_{ij} is the Coriolis tensor. The Coriolis forces are neglected in these developments, although they may be of relevance, since we are dealing with very large domains of several hundred kilometers of size, in general, and for phenomena observed over a very large time scale. This is being presently assessed.

Indicial notation is used, for $i, j = 1, 2, 3$ representing the directions (x, y, z), derivatives given by a comma and repeated indices indicating a sum. In the subsequent developments, indices l, k represent only the horizontal directions (x, y). A dot indicates derivative with respect to time.

3 FORMULATION OF A TWO-LAYER PROBLEM

The continuity Eq. (1) is applied to the flow of

- a layer of sediments flowing with velocity $\mathbf{q}^s(z, y, z, t)$ between a rigid bed given by $z = Z(x, y)$ and an intermediary surface given by $z = H^s(x, y, t)$ between the sediment stream and the sea water, and
- a layer of sea water, whose lower surface is $z = H^s(x, y, t)$ and upper surface is $z = H^w(x, y, t) \equiv H^w = \text{constant}$, and flowing with velocity $\mathbf{q}^w(z, y, z, t)$.

This is illustrated in Fig. 1 together with some relations that are introduced [but not demonstrated (Dumont, 2014)] in the subsequent developments.

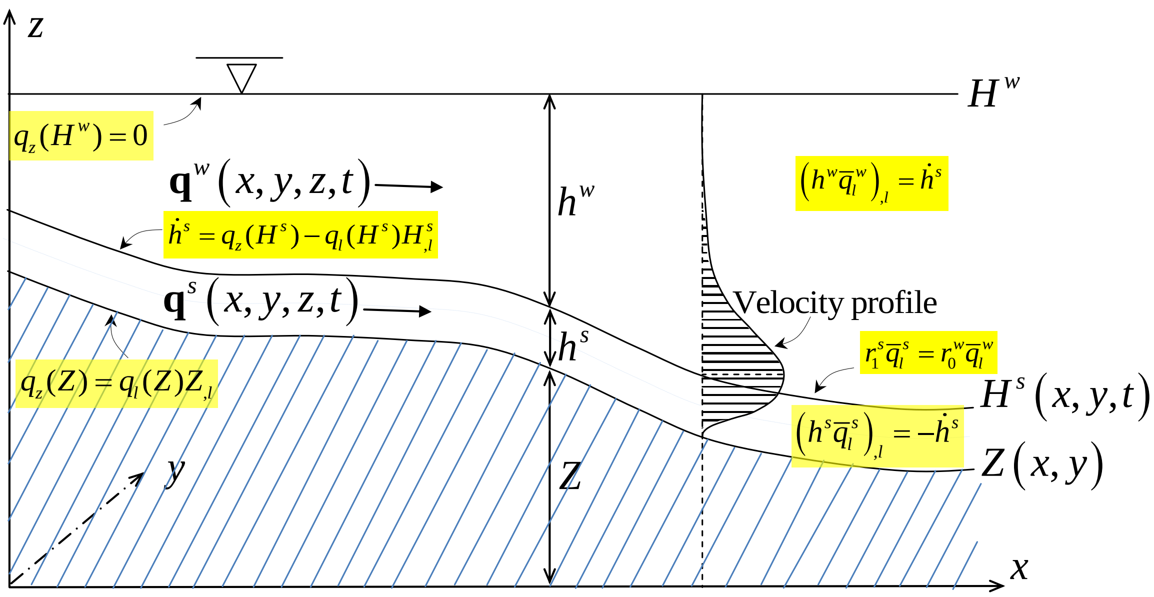

Figure 1: Representation of the bed profile $z = Z(x, y)$ and the surface $z = H^s(x, y, t)$ between sediment flow and sea water of level $H^w = \text{constant}$ together with the obtained continuity equations.

3.1 The concept of vertically averaged horizontal velocities

Since the flow is predominantly horizontal inside the sediment layer, the velocity profile across the sediment layer is assumed as constant, only with its intensity varying as a function of the coordinates (x, y, t):

$$q_l(x, y, z, t) = r(s)\bar{q}_l(x, y, t) \tag{4}$$

where $\bar{q}_l(x, y, t)$ is the averaged fluid flow and $r(s)$ is the velocity profile defined in terms of the argument

$$s \in [0, 1] = (z - Z)/h \tag{5}$$

and normalized such that

$$\int_0^1 r(s)ds = 1. \tag{6}$$

The term

$$\beta = \int_0^1 r^2(s)ds \tag{7}$$

will reflect the effect of the velocity profiles of sediment and water layers in Eqs. (17), (18) and (22). As illustrated in Fig. 1, the function $r(s)$ is chosen in such a way that $r(0)$ is close to zero and $r(1)$ has the maximum value in $s \in (0, 1)$ in order to account for the drag caused by the sea bed, although other possibilities of interpretation are not excluded (Tetzlaff & Harbaugh, 1989). A derivative with respect to s is indicated by a prime.

As proposed (Tetzlaff & Harbaugh, 1989), $r(s)$ represents a velocity profile that does not change with x , y or t. On the other hand, the argument s defined in Eq. (5) is dependent on all three arguments. This is a contradiction, to be circumvented by the understanding that the concept of a velocity profile is just an approximation of the actual three-dimensional phenomenon. Then, although it is licit to write from Eq. (5) that

$$\frac{\partial r(s(z))}{\partial z} = \frac{1}{h}\frac{dr(s)}{ds} \equiv \frac{r'}{h} \tag{8}$$

all derivative manipulations of $r(s)$ involving the variables x , y or t must be avoided in the subsequent mathematical developments,

3.2 Geometric and continuity relations

The thicknesses of the sediment and water layers are given as

$$h^s = H^s - Z; \quad h^w = H^w - H^s \Rightarrow h^s + h^w = H^w - Z \equiv h \tag{9}$$

The condition of no flow perpendicular to $Z(x, y)$ on the bottom of the sediment is expressed as

$$q_z(Z) = q_l(Z)Z_{,l} \tag{10}$$

The boundary condition for the flow on the intermediary surface $z = H^s$ between sediment and sea water is

$$h^s = q_z(H^s) - q_l(H^s)H^s_{,l} \tag{11}$$

The boundary condition on the assumed free surface of the sea water is

$$q_z(H^w) = 0 \tag{12}$$

Moreover, the equation for the sediment flow in the vertical direction is expressed as

$$(h_s\bar{q}^s_l)_{,l} = -\dot{h}^s \tag{13}$$

while, for the water flow in the vertical direction,

$$(h_w\bar{q}^w_l)_{,l} = \dot{h}^s \tag{14}$$

and a compatibility condition of sediment and water flows at $z = H^s$ is established as

$$r^s_1\bar{q}^s_l = r^w_0\bar{q}^w_l \tag{15}$$

For clarity, these continuity equations are represented in yellow in Fig. 1.

Moreover, as illustrated in Fig. 1, it is possible to assume for the velocity profiles of the sediment and water layers without much loss of generality that, for $s = 0$ and $s = 1$,

$$\begin{aligned} r^s_0 &= r^w_1 = 0 \\ r'^s_0 &= r'^s_1 = r'^w_0 = r'^w_1 = 0 \end{aligned} \tag{16}$$

3.3 Momentum equations.

After some tedious developments, the momentum Eq. (2) becomes expressed for the sediment and water layers as

$$\frac{\partial(h^s\bar{q}^s_l)}{\partial t} + (h^s\bar{q}^s_k\bar{q}^s_l\beta^s)_{,k} = gh^sH^s_{,l}\left(\frac{\rho^w}{\rho^s} - 1\right) + \frac{\mu^s}{\rho^s}\left[\left(\left(h^s - H^sr^s_1\right)\bar{q}^s_l\right)_{,kk} + H^sr^s_0\bar{q}^s_{l,kk}\right] \tag{17}$$

$$\frac{\partial(h^w\bar{q}^w_l)}{\partial t} + (h^w\bar{q}^w_k\bar{q}^w_l\beta^w)_{,k} = \frac{\mu^w}{\rho^w}\left[\left(\left(h^w + H^sr^w_0\right)\bar{q}^w_l\right)_{,kk} - H^sr^w_0\bar{q}^w_{l,kk}\right] \tag{18}$$

The four equations above ($l = 1, 2$) together with the geometric and compatibility Eqs. (9) and (15) – and given consistent boundary and initial conditions – build a system of equations that must be sufficient to solve for the six basic unknowns of the problem: $\bar{q}^s_l$, $\bar{q}^w_l$, h^s, h^w. However, consistently handling all these equations is not a simple matter, which requires a careful approach.

3.4 A first solution development of the proposed equations

Equations (17) and (18) can be combined as

$$\begin{aligned}(h^s\bar{q}_l^s + h^w\bar{q}_l^w)_{,kk} = \;& \frac{\rho^s}{\mu^s}\left[\partial\left(h^s\bar{q}_l^s\right)/\partial t \;+ \left(h^s\bar{q}_k^s\bar{q}_l^s\beta^s\right)_{,k} - gh^sH_{,l}^s\left(\frac{\rho^w}{\rho^s}-1\right)\right] \\ + \;& \frac{\rho^w}{\mu^w}\left[\partial\left(h^w\bar{q}_l^w\right)/\partial t \;+ \left(h^w\bar{q}_k^w\bar{q}_l^w\beta^w\right)_{,k}\right]\end{aligned} \tag{19}$$

Deriving this latter equation with respect to the direction l and adding, the term on the left-hand side becomes void and it results

$$\begin{aligned}&\frac{\rho^s}{\mu^s}\left[-\ddot{h}^s + \beta^s\Big(-\dot{h}^s\bar{q}_l^s + h^s\bar{q}_{l,k}^s\bar{q}_k^s\Big)_{,l} - g\big(h^sH_{,l}^s\big)_{,l}\left(\frac{\rho^w}{\rho^s}-1\right)\right] \\ &+\frac{\rho^w}{\mu^w}\left[\ddot{h}^s + \beta^w\Big(\dot{h}^s\bar{q}_l^w + h^w\bar{q}_{l,k}^w\bar{q}_k^w\Big)_{,l}\right] = 0\end{aligned} \tag{20}$$

Since h^s and h^w are linked by Eq. (9), the above equation is a second-order, non-linear differential equation to evaluate either h^s or h^w in the frame of an iterative scheme to be proposed.

3.5 A second solution development of the proposed equations

A formulation of the proposed problem is attempted by expressing the equivalent horizontal flows in terms of a potential function ϕ,

$$\begin{aligned}h^s\bar{q}_x^s + h^w\bar{q}_x^w &= \phi_{,y} \\ h^s\bar{q}_y^s + h^w\bar{q}_y^w &= -\phi_{,x}\end{aligned} \tag{21}$$

which automatically satisfies the sum of Eqs. (13) and (14). As proposed, $\phi_{,y}$ and $-\phi_{,x}$ have the meaning of total sediment and water flows in the horizontal x and y directions, respectively. Then, the momentum Eqs. (17) and (18) result into the more tractable set of stream line – vorticity equations

$$\begin{aligned}\phi_{,ll} &= -\omega \\ \omega_{,ll} &= -\frac{\rho^s}{\mu^s}\left[\dot{\omega}^s + \beta^s\left[\dot{\omega}^s\bar{q}_k^s + h^s\left(\bar{q}_{k,y}^s\bar{q}_x^s - \bar{q}_{k,x}^s\bar{q}_y^s\right)\right]_{,k} - g\left[h_{,y}^sZ_{,x} - h_{,x}^sZ_{,y}\right]\left(\frac{\rho^w}{\rho^s}-1\right)\right] \\ &\quad -\frac{\rho^w}{\mu^w}\left[\dot{\omega}^w + \beta^w\left[\dot{\omega}^w\bar{q}_k^w + h^w\left(\bar{q}_{k,y}^w\bar{q}_x^w - \bar{q}_{k,x}^w\bar{q}_y^w\right)\right]_{,k}\right]\end{aligned} \tag{22}$$

where $\omega = \omega^s + \omega^w$ is the sum of the vorticities of the set of sediment and water layers:

$$\begin{aligned}\omega^s &= \left(h^s\bar{q}_y^s\right)_{,x} - \left(h^s\bar{q}_x^s\right)_{,y} \\ \omega^w &= \left(h^w\bar{q}_y^w\right)_{,x} - \left(h^w\bar{q}_x^w\right)_{,y}\end{aligned} \tag{23}$$

3.6 Proposed solution attempt

According to the proposed solution layout, Eqs. (22) and (20) can be expressed in a stream line-vorticity formulation of the classical Navier-Stokes equations plus a third scalar equation in terms of h^s (developments not shown):

$$\begin{aligned} \nabla^2\phi &= -\omega \\ \nabla^2\omega &= f(\phi, h^s) \\ \nabla^2 h^s &= g(\phi, h^s) \end{aligned} \tag{24}$$

only bearing in mind that the non-linear functions $f(\phi, h^s)$ and $g(\phi, h^s)$ are sums of several products of derivatives of ϕ up to the third order. This makes the above equations solvable only in the frame of an iterative procedure for which convergence cannot be demonstrated.

A robust solution strategy must be developed for the above equations, since the physical domain to which they are meant to apply may be very irregular and also multiply connected as different sea level conditions may be deemed of interest in the stratigraphic assessment of a sedimentary basin.

These equations are not further developed, since several aspects of practical as well as of numerical relevance must be first dealt with for a feasibility assessment of the proposed formulation.

4 THE EXPEDITE BOUNDARY ELEMENT METHOD

The expedite boundary element method, a simplified, variationally-based formulation, has been well explained by Dumont & Aguilar (2012a, 2012b). For the present case of a potential problem, it relies on the assumption that a given potential function ϕ and its gradients $\phi_{,l}$ inside a domain can be described in terms of a series of point source parameters q^*_m applied along the boundary plus some arbitrary particular solution ϕ^p,

$$\begin{aligned} \phi &= (\phi^*_m + C_m)\, q^*_m + \phi^p \\ \phi_{,l} &= \phi^*_{m,l} q^*_m + \phi^p_{,l} \end{aligned} \tag{25}$$

where ϕ^*_m is a fundamental solution of the corresponding differential equation of the problem. In the present case, $\bigtriangledown^2\phi^*_m = 0$ except for the point of application of q^*_m, when ϕ^*_m becomes undetermined. Moreover, ϕ^*_m is obtained except for a constant C_m (Dumont & Aguilar, 2012a, 2012b). This belongs to the basic theory of the conventional boundary element method only bearing in mind that in a variational formulation ϕ^*_m is used as a numerical approximation of the actual problem and not just as a weighting function.

Assigning subscripts D and N to subvectors of nodal potentials $\mathbf{d}$ and equivalent nodal gradients $\mathbf{p}$ to characterize whether the boundary conditions are of Dirichlet or Neumann type, the final matrix equation system of the expedite boundary element method is expressed as

$$\begin{bmatrix} \mathbf{U}^*_N \\ \mathbf{U}^*_D \end{bmatrix} \mathbf{p}^* = \begin{Bmatrix} \mathbf{d}_N - \mathbf{d}^p_N \\ \mathbf{d}_D - \mathbf{d}^p_D \end{Bmatrix}, \quad \begin{bmatrix} \mathbf{H}^{\mathrm{T}}_N \\ \mathbf{H}^{\mathrm{T}}_D \end{bmatrix} \mathbf{p}^* = \begin{Bmatrix} \mathbf{p}_N - \mathbf{p}^p_N \\ \mathbf{p}_D - \mathbf{p}^p_D \end{Bmatrix} \tag{26}$$

where the quantities with superscript p stand for nodal potentials or gradients belonging to the assumed, arbitrary particular solution of the problem. $\mathbf{H}$ is the double-layer potential matrix and $\mathbf{U}^*$ represents the fundamental solutions ϕ_m^* evaluated at the boundary nodal points. The equations above can be firstly solved for $\mathbf{p}^*$ in terms of the known nodal quantities, provided that the problem is well posed, with the subsequent evaluation of the remaining boundary potentials and gradients:

$$\begin{bmatrix} \mathbf{H}_N^{\mathrm{T}} \\ \mathbf{U}_D^* \end{bmatrix} \mathbf{p}^* = \begin{Bmatrix} \mathbf{p}_N - \mathbf{p}_N^p \\ \mathbf{d}_D - \mathbf{d}_D^p \end{Bmatrix} \Rightarrow \begin{bmatrix} \mathbf{d}_N \\ \mathbf{p}_D \end{bmatrix} = \begin{Bmatrix} \mathbf{d}_N^p \\ \mathbf{p}_D^p \end{Bmatrix} + \begin{bmatrix} \mathbf{U}_N^* \\ \mathbf{H}_D^{\mathrm{T}} \end{bmatrix} \mathbf{p}^* \tag{27}$$

The results at internal points are obtained directly by using Eq. (25). Results close to or at nodal points can also be obtained (Dumont & Aguilar, 2012a, 2012b). The implemented 2D boundary element code works with linear, quadratic or cubic elements.

5 INTERACTION WITH A FINITE DIFFERENCE SCHEME

A finite-difference (FD) numerical discretization would per se be able to deal with the problem proposed in Eq. (24), particularly because it can directly handle the highly non-linear domain terms represented by $f(\phi, h^s)$ and $g(\phi, h^s)$. However, dealing with boundary conditions for an arbitrarily shaped domain is not a simple task in terms of finite differences. The chosen strategy is to use finite differences to solve Eq. (24) for a rectangular domain that encloses the actual domain of interest, and then apply the results as the particular solution of the boundary element Eq. (27), which can accurately take boundary conditions into account no matter how irregular a domain can be. The implemented 2D code works with either quadratic of quartic FD schemes.

Although the particular solution to be used in Eq. (27) can be in principle arbitrary, serious round-off error and convergence issues occur when it differs too much from the actual solution one is trying to reproduce. In fact, it is advised to choose the particular solution as close as possible to the actual one so as to minimize the correction needed in terms of the boundary-element vector of parameters $\mathbf{p}^*$, as obtained in Eq. (27).

Let the FD matrix of either of Eq. (24) be expressed as

$$\mathbf{A}\mathbf{x} = \mathbf{b} \tag{28}$$

where $\mathbf{b}$ collects the right-hand terms known at a given iteration and $\mathbf{x}$ is the vector of improved solutions we are looking for. Prior to introducing boundary conditions, $\mathbf{A}$ is symmetric and with a regular banded pattern, since the mesh is rectangular. There are several possibilities of proceeding with the solution, as proposed in the literature (Elghaoui & Pasquetti, 1999; Le *et al.*, 2008). Since, for an embedded irregular domain, the boundary of the regular mesh is not part of the actual problem, instead of introducing boundary conditions we introduce nodal restrictions in the mesh interior, formally expressed as

$$\mathbf{P}\mathbf{x} = \mathbf{c} \tag{29}$$

where $\mathbf{P}$ is a rectangular, very sparse, matrix whose rows represent imposed restrictions on nodal potentials that are close to the boundary element nodes of the irregular domain. This is illustrated in Fig. 2, where there is on the right an irregularly-shaped, multiply connected domain embedded in a rectangular mesh. As visualized in the inset on the left, after scanning the whole FD mesh (a process that is carried out only once), the FD nodes that are closest to the boundary and just outside the domain of interest are singled out for introduction of the restrictions represented by Eq. (29), by attributing to these nodes the boundary condition of the closest boundary element node, as indicated by the arrows in the inset. Since the singled-out FD nodes and the boundary element nodes do not necessarily coincide, such attribution is only an approximation, which is just fine, as we are dealing with a particular solution that is in principle arbitrary. For Dirichlet boundary conditions, as illustrated in Fig. 2, the corresponding row of **P** just indicates that the FD node potential is equal to the closest, assigned boundary element node potential. For Neumann boundary conditions, the corresponding row of **P** represents the FD scheme of some prescribed normal gradient. Observe that the boundary element implementation works with equivalent nodal normal gradients whereas the FD scheme makes use of gradients in the coordinate directions, which requires some transformations between the represented quantities.

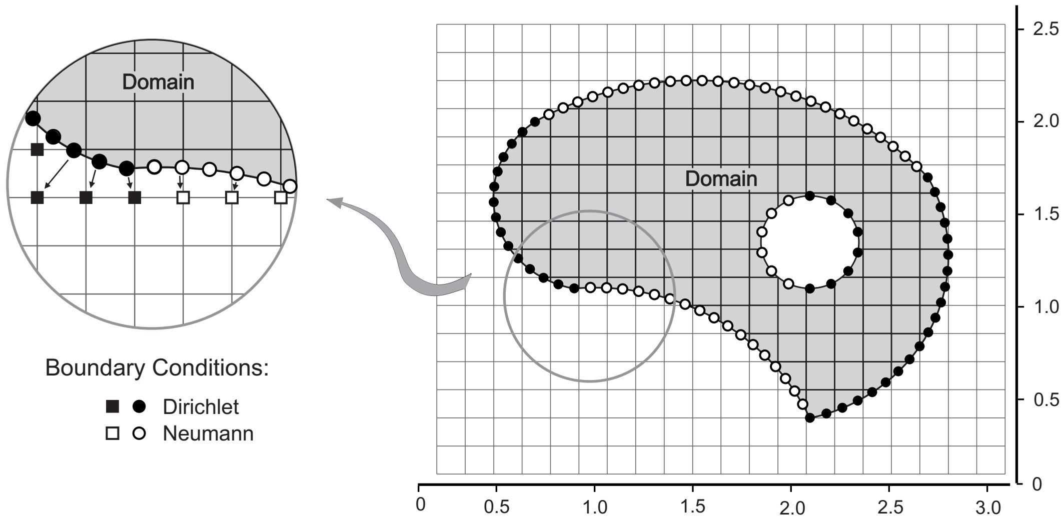

Figure 2: Irregularly shaped, multiply connected domain (right) discretized with 92 linear boundary elements embedded in a 21x17 FD mesh for the solution of the numerical example of Eq. (32) with indicated mixed boundary conditions. The inset helps to visualize how the boundary conditions of the auxiliary FD mesh are prescribed.

The solution of Eq. (28) submitted to the restrictions given by Eq. (29) can be best obtained in terms of least squares, which ultimately leads to

$$\left(\mathbf{A}^{\mathrm{T}}\mathbf{A} + \mathbf{P}^{\mathrm{T}}\mathbf{P}\right)\mathbf{x} = \mathbf{A}^{\mathrm{T}}\mathbf{b} + \mathbf{P}^{\mathrm{T}}\mathbf{c} \tag{30}$$

with the system matrix symmetric, positive definite and banded. This system can be pre-solved and stored (using Cholesky decomposition, as implemented) in order to speed up the numerical process along the long cycle of iterations. Once the solution vector **x** is obtained in Eq. (30) the corresponding boundary node results to be fed into Eq. (27) are accurately interpolated in terms of the enveloping FD molecules.

6 ITERATIVE SOLUTION

Equation (24) is solved iteratively for homogeneous Dirichlet boundary conditions in terms of the vorticity ω [see Ghia *et al.* (1982) for a discussion on the subject] and the boundary conditions assigned to the stream function ϕ that can best reproduce the water plus sediment inflow or outflow conditions, according to Eq. (21). We start with the first of Eq. (24) setting $\omega = 0$, thus obtaining a first guess of ϕ, to enter the second equation and find an improvement for ω and, and then for h^s in the third equation, successively iterating until the difference between previous and evaluated nodal values in the domain of interest do not differ more than a given tolerance. Stability and convergence of the algorithm cannot be demonstrated. Relaxation is usually resorted to in such an iterative scheme, which in general consists in expressing the improved result of a given iteration as $x_{n+1} = (1-\alpha)x_n + \alpha f(x_n)$ instead of $x_{n+1} = f(x_n)$, where under-relaxation occurs for $0 < \alpha < 1$ and there is an over-relaxation in the case of $\alpha > 1$.

7 A NUMERICAL EXAMPLE

The functions

$$\begin{aligned} u(x,y) &= \sin xy \\ v(x,y) &= \sin\frac{x\pi}{2}\cos\frac{y\pi}{3} \\ w(x,y) &= \frac{-x^2y+10}{15} \end{aligned} \tag{31}$$

are the solution of the coupled, non-linear equation system

$$\begin{aligned} \nabla^2 u &= -v^2 + \sin^2\frac{\pi x}{2}\cos^2\frac{\pi y}{3} - y^2\sin xy - x^2\sin xy \\ \nabla^2 v &= u^2 + w^2 - \sin^2 xy + \left(\frac{x^2y}{15} - \frac{2}{3}\right)^2 - \frac{13\pi^2}{36}\sin\frac{x\pi}{2}\cos\frac{y\pi}{3} \\ \nabla^2 w &= uw + \left(\frac{x^2y}{15} - \frac{2}{3}\right)\sin xy - \frac{2y}{15} \end{aligned} \tag{32}$$

These equations are an artifact of a non-linear, coupled system of equations to be dealt with according to the proposed solution strategy for Eq. (24). A numerical problem is proposed as the solution of Eq. (32) in the irregular, multiply connected domain shown on the right of Fig. 2, for mixed boundary conditions imposed at the indicated points according to the known solutions in Eq. (31). The outer boundary of Fig. 2 consists of four linked arc segments with corner points of coordinates (0.9, 1.1), (2.1, 0.4), (2.7, 1.7) and (0.7, 2.0) and radii 1.2, 0.9, 1.6 and 0.5, respectively, in lengths units; there is also a circular hole of radius 0.25 centered in (2.1, 1.35). For simplicity, Dirichlet and Neumann boundary conditions are prescribed on the same subboundaries for all three equations, as indicated in Fig. 2. The proposed problem does not have the high derivatives of Eq. (22) but on the other hand requires that all three equations be solved iteratively. Since there are several convergence and stability issues to be dealt with, the solution of the proposed problem is useful as an apprenticeship of how to deal with this kind of problems, since it is sufficiently general and there is an analytical solution to compare with. Figure 2 represents the coarsest of four boundary element (BE) meshes embedded in finite difference (FD) meshes, as given in Table 1.

As shown in Table 2, up to eight iterations have been required for all implemented meshes to achieve a convergence error of 10^{-9} in terms of potential results at the FD nodal points in the domain of interest, with a variable, but decreasing, number of iterations locally required to solve each equation also for a convergence error tolerance of 10^{-9}. The analytical values (dots) and the numerical results (circles) of the three functions of Eq. (31) are plotted in Fig. 3 for the coarsest mesh both in the domain and along the boundary. In these plots, which are each differently rotated for the sake of visualization, analytical and numerical values are indistinguishable from each other.

Table 1: Discretization meshes for the analysis of the problem proposed in Eq. (32) of the domain of Fig. 2.

	Number of d.o.f. of the FD mesh	Number of d.o.f of the BE mesh	Total Number of d.o.f
Mesh#1	$21\text{x}17 = 357$	$78 + 14 = 92$	449
Mesh#2	$41\text{x}33 = 1353$	$156 + 28 = 184$	1537
Mesh#3	$61\text{x}49 = 2989$	$234 + 42 = 276$	3265
Mesh#4	$81\text{x}65 = 5265$	$312 + 56 = 368$	5633

Table 2: Number of iterations needed to locally solve each one of Eq. (32) as the global iteration advances.

	Mesh #1			Mesh #2			Mesh #3			Mesh #4		
Iter.	Eq.1	Eq.2	Eq.3	Eq.1	Eq.2	Eq.3	Eq.1	Eq.2	Eq.3	Eq.1	Eq.2	Eq.3
1	2	2	14	2	2	14	2	2	14	2	2	14
2	2	2	10	2	2	11	2	2	11	2	2	11
3	2	2	9	2	2	9	2	2	10	2	2	10
4	2	2	7	2	2	7	2	2	7	2	2	7
5	2	2	6	2	2	6	2	2	6	2	2	6
6	2	2	4	2	2	4	2	2	4	2	2	4
7	2	2	2	2	2	2	2	2	2	2	2	2
8	1	1	1	1	1	1	1	1	1	2	1	1

Both the convergence errors of the iterative process and the actual errors, obtained by comparing the results with the analytical values of Eq. (31), are plotted on the left of each row of graphs in Fig. 4 for Mesh # 4, as given in Table 1, to show that, for a given mesh, the actual errors do not decrease when a certain threshold is achieved. No relaxation was used to arrive at the displayed results. Is was observed, for the present numerical example, that under-relaxation may lead to a smaller number of iterations, as a whole, but cannot contribute to the improvement of results, which can only be achieved by increasing the mesh refinement, as shown in the convergence graphs on the right in Fig. 4 for each one of Eq. (32).

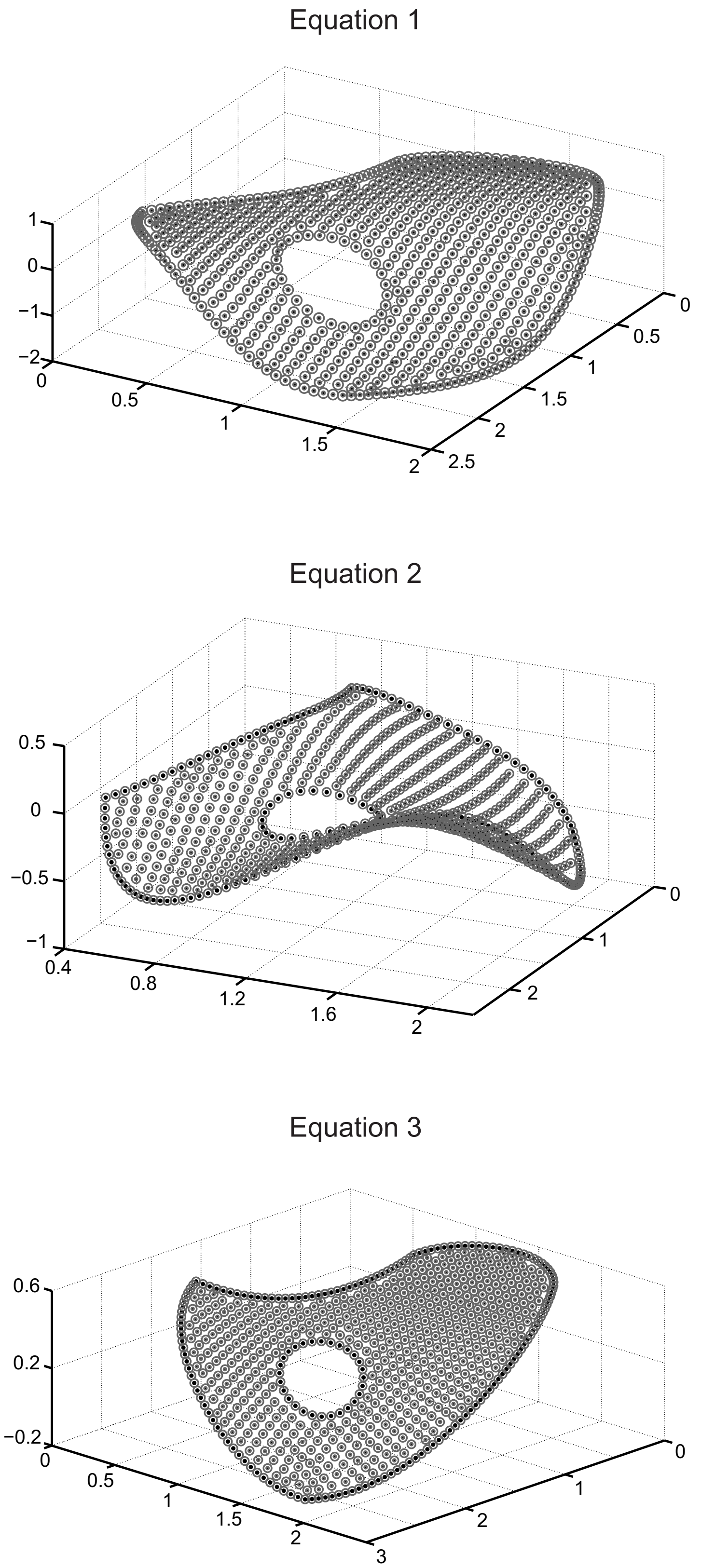

Figure 3: Numerical (circles) and analytical (dots) results for the coarsest mesh (Mesh # 1 in Table 1).

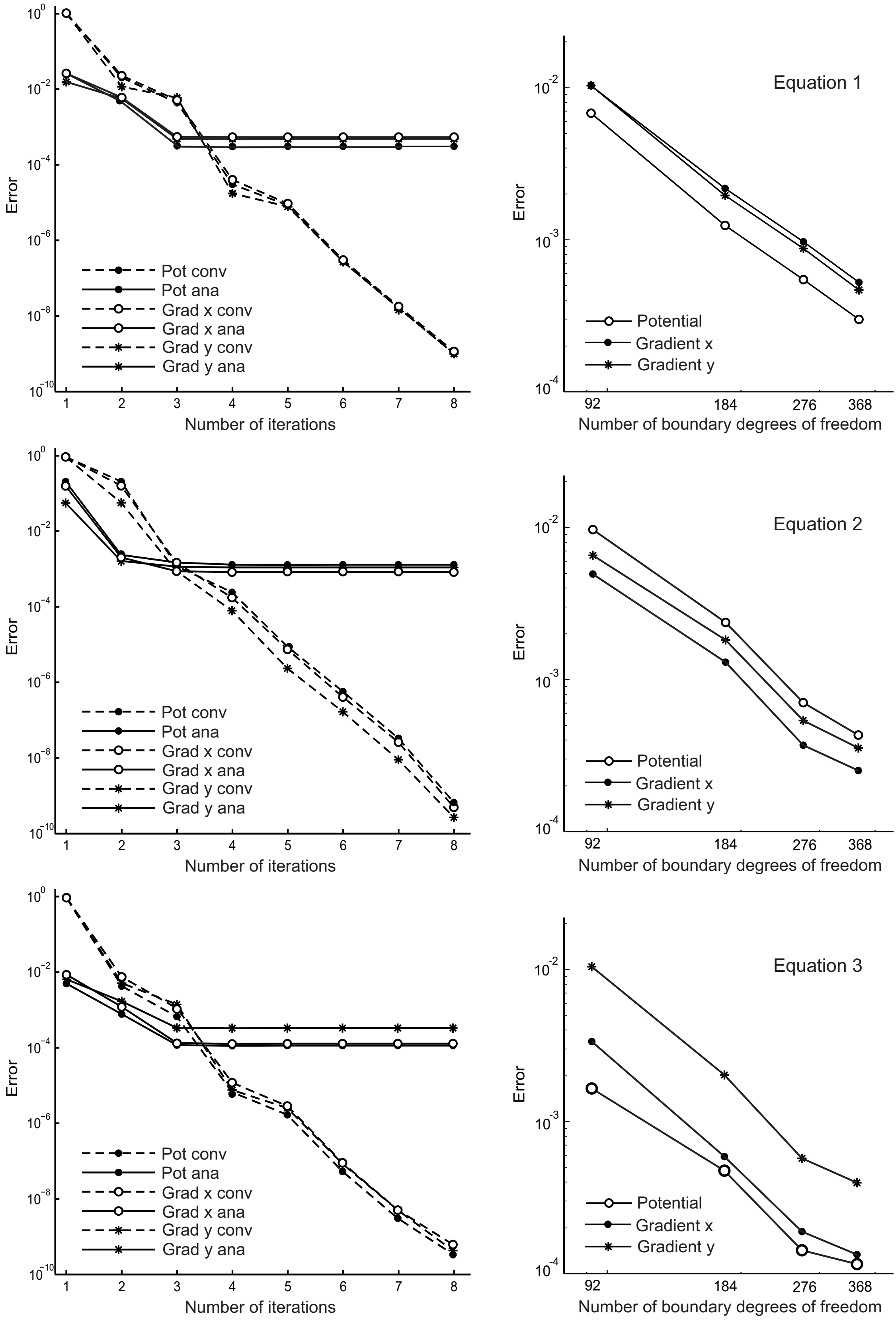

Figure 4: (Left) local convergence (conv) and actual (ana) errors for all three equations of Eq. (32), as obtained for Mesh # 4 in Table 1. (Right) actual errors after convergence for each one of the four meshes.

8 SIMPLIFIED DEVELOPMENTS FOR A ONE-LAYER PROBLEM

Although both mechanically and mathematically feasible, the equations outlined in Section 3 are too general to deal with in practical applications, as, for instance, one would need to prescribe boundary and initial conditions for the sea water as well as for the sediment layer and then look for the solution of this intricated problem. There are two possibilities of particularizing the proposed general equations. The first possibility – a work in progress – consists in simply assuming that the sea water flows with prescribed velocity: the case of zero velocity would be the first attempt. However, owing to space restriction this possibility is not dealt with in this manuscript.

The second and simplest (actually too simple) possibility is the subject of the present section and consists in particularizing the equations for a single layer of a mixture of water and sediments, which would be applicable to a shallow sea.

For the one-layer problem, Fig. 1 simplifies to Fig. 5, and no superscript is then needed to characterize the quantities involved in the formulation, as the unknowns all refer to the sediment layer. According to that, the 2D continuity Eqs. (13) and (14) become simply

$$(h\bar{q}_l)_{,l} = 0 \tag{33}$$

Where h – the sea depth – is no longer one of the problem's unknowns. The 2D momentum equation becomes expressed, according to Fig. 5, as a particularization of Eq. (19):

$$h\dot{\bar{q}}_l + (h\bar{q}_k\bar{q}_l\beta)_{,k} = \frac{\mu}{\rho}(h\bar{q}_l)_{,kk} \tag{34}$$

The solution attempt in terms of a potential function is simply, instead of Eq. (21),

$$\begin{aligned} h\bar{q}_x &= \phi_{,y} \\ h\bar{q}_y &= -\phi_{,x} \end{aligned} \tag{35}$$

and, from Eq. (22),

$$\dot{\phi}_{,ll} + \beta(\phi_{,l}\bar{q}_k)_{,lk} = \frac{\mu}{\rho}\phi_{,llkk} \tag{36}$$

This fourth order equation can be transformed into the following two equations:

$$\begin{aligned} &\phi_{,ll} = -\omega \\ &\frac{\mu}{\rho}\omega_{,kk} = \dot{\omega} - \beta(\phi_{,l}\bar{q}_k)_{,lk} \end{aligned} \tag{37}$$

which are easier to deal with mathematically. The expanded version of these two equations is

$$\frac{\partial^2\phi}{\partial x^2} + \frac{\partial^2\phi}{\partial y^2} = -\omega \tag{38}$$

$$\left(\frac{\partial^2\omega}{\partial x^2} + \frac{\partial^2\omega}{\partial y^2}\right) = \frac{\rho}{\mu}\dot{\omega} - \frac{\rho\beta}{\mu}\left[(\phi_{,x}\bar{q}_x)_{,xx} + (\phi_{,x}\bar{q}_y)_{,xy} + (\phi_{,y}\bar{q}_x)_{,xy} + (\phi_{,y}\bar{q}_y)_{,yy}\right] \tag{39}$$

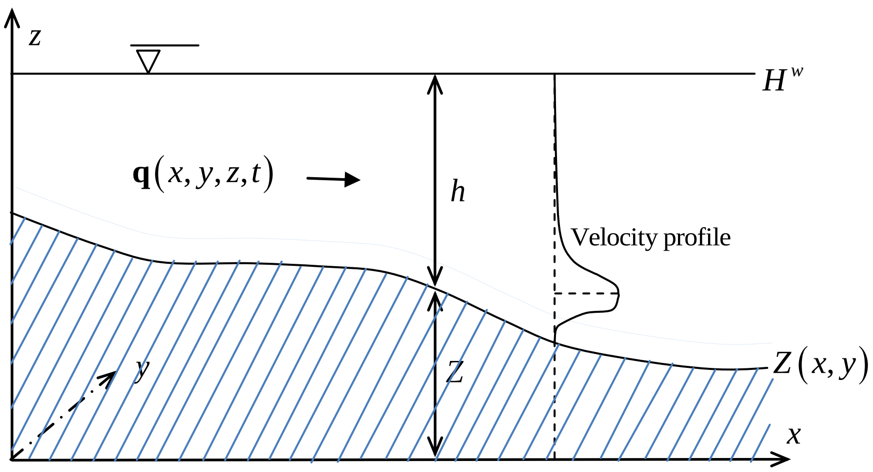

Figure 5: Representation of the bed profile $z = Z(x, y)$ for the one-layer flow of water and sediment.

In the following, these equations are tested for a rectangular domain with a typical sea bottom relief and considering different boundary conditions. Since this is a regular domain, only a finite-difference scheme (developed in C++) was applied, with boundary conditions introduced as restrictions exactly as given in Eqs. (28-30).

The sea relief (not an actual one) is generated using Petrobras' own code StratBR with a 64×45 rectangular grid ($\Delta_x = 2.790km$ and $\Delta_y = 2.658km$), as depicted in Fig. 6. The boundary conditions are given as prescribed constant normal inflow ($q_n = 1$ in consistent units) along all 45 cells on the northeast edge and constant normal outflow ($q_n = 3$) on 15 cells of the opposite edge, as indicated in the figure. There is no flow along the remaining boundary parts. For this model, the sea level is given as $H^w = 2.95km$) so that an island is formed close to the westernmost corner. The streamline results are shown in Fig. 7, which are qualitatively satisfactory. Observing the irregular boundary along the island one may conclude that actually an interaction with the boundary element model would be required.

CONCLUSIONS

The basic scope of the presented developments is the implementation of a computational model for the simulation of transport, deposition and erosion phenomena in sedimentary basins by considering the variation in time and space of a sediment layer that flows on the sea bottom. The specific problems solved in the present paper still have steady-state nature, since convergence issues must be first adequately addressed before including the time effect and eventual property changes of the transported material. It is not possible to demonstrate mathematically that the proposed algorithms converge unconditionally. Several examples have already been tested involving the multiplication of high-order derivatives, as they appear in Eq. (22), which showed that the critical issue is the adequate selection of the relaxation factor to guarantee stability and convergence of the iterative process. Moreover, uncontrollable round-off errors may occur if the finite-difference particular solution related to the domain, non-linear terms is too far apart from the sought solution. This was the reason to introduce the matrix of restrictions of Eq. (29), which has turned the whole iterative procedure reliable and cost-effective – at least

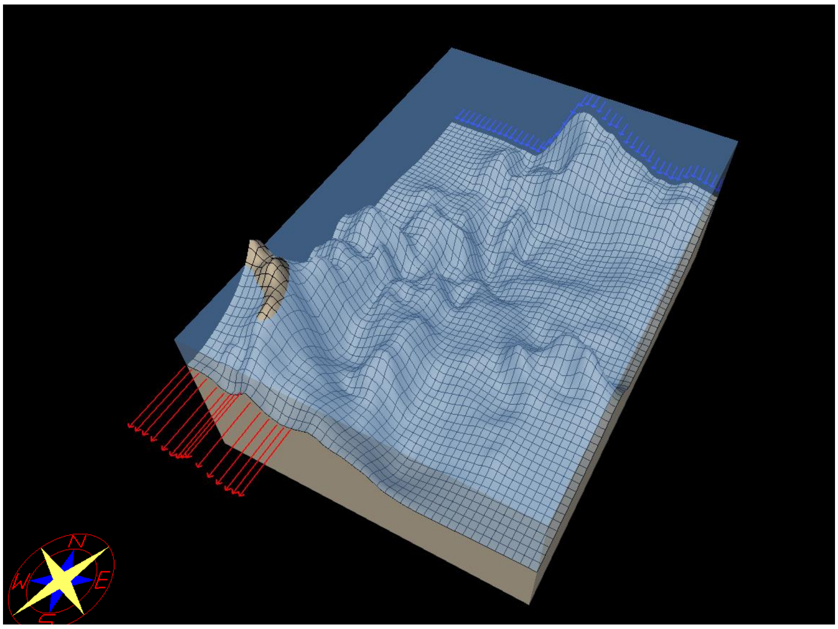

Figure 6: 64×45 rectangular grid for the numerical simulation of Section 8.

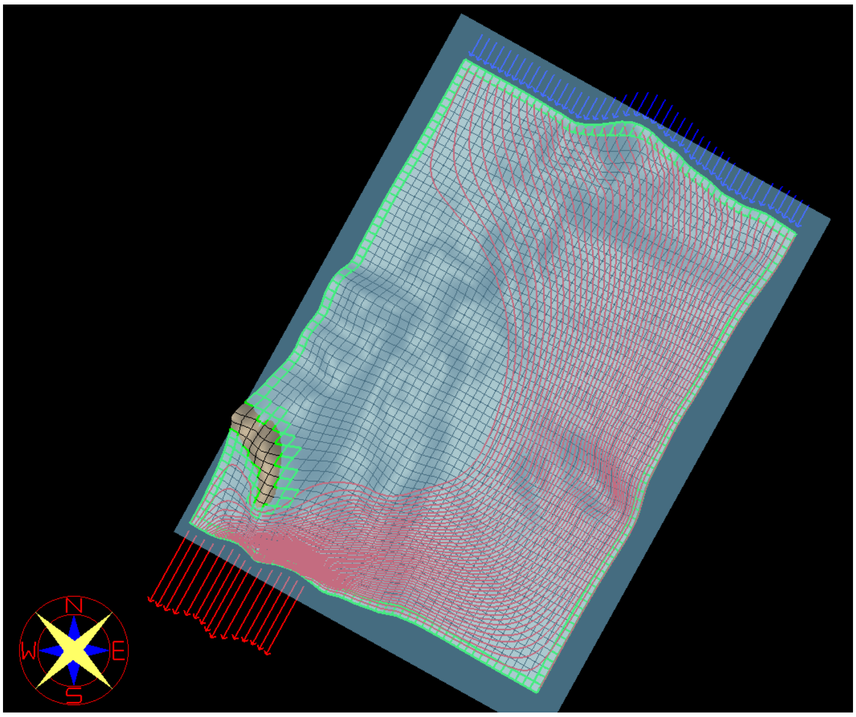

Figure 7: Stream line results for the problem proposed in Fig. 6.

for the numerical experiments carried out so far. The use of a quartic finite-difference scheme enables the consideration of products of high-order derivatives, so that no linearization (Sheu & Lin, 2004) of the equations has turned out necessary. The proposed embedded formulation also seems more straightforward to apply than techniques such as the one described by Šarler & Kuhn (1999). Out of the general formulation laid down in Section 3 a few simplifications seem not only possible but also mechanically more realistic, as briefly described in Section 8.

The most promising formulation consists in considering the two-layer problem in which the sea water has zero prescribed flow. Moreover, the influence of the Coriolis force is being presently assessed.

ACKNOWLEDGEMENTS

This work is part of a research project sponsored by Petrobras. The authors are also thankful to the Brazilian funding agencies CAPES, CNPq and FAPERJ.

REFERENCES

Biros, G., Ying, L., & Zorin, D., 2002. The embedded boundary integral method (EBI) for the incompressible Navier-Stokes equations. *IABEM 2002 – Symposium of the International Association for Boundary Element Methods*, 12 pp., UT Austin.

Buzbee, B. L., Dorr, F. W., George, J. A., & Golub, G. H., 1971. The direct solution of the discrete Poisson equation on irregular regions. *SIAM Journal of Numerical Analysis*, vol. 8, pp. 722-736.

Dumont, N. A., 2014. Simulating Clastic Sedimentation-Flow of a Sediment Layer on the Sea Bed. Internal Report, PUC-Rio, Brazil.

Dumont, N. A. & Aguilar, C. A., 2012a. The best of two worlds: The expedite boundary element method. *Engineering Structures*, vol. 43, pp. 235-244.

Dumont, N. A. & Aguilar, C. A., 2012b. On a strategy to implement a fast and expedite boundary element method. *Advances in Boundary Element Techniques XIII*, eds. P. Prochazka and M. H. Aliabadi, Prague, Czech Republic, pp. 295-302.

Dumont, N. A., Mamani, E. Y., Aguilar, C. A. & Peixoto, H. F. C., 2015. An embedded variationally-hybrid boundary element formulation for the solution of Navier Stokes equations over irregular two-dimensional domains. In Mantic, V., Saez, A., & Aliabadi, M. H., eds, *Advances in Boundary Element Techniques XVI*, pp. 223-230, EC, Ltd, UK.

Elghaoui, M., & Pasquetti, R., 1999. Mixed spectral-boundary element embedding algorithms for the Navier-Stokes equations in the vorticity-stream function formulation. *Journal of Computational Physics*, vol. 153, pp. 82-100.

Ghia, U., Ghia, K. N. & Shin, C. T., 1982. High-Re solutions for incompressible flow using the Navier-Stokes equations and a multigrid method. *Journal of Computational Physics*, vol. 48, pp. 387-411.

Le, D. V., Khoo, B. C. & Lim, K. M., 2008. An implicit-forcing immersed boundary method for simulating viscous flows in irregular domains. *Comput. Methods Appl. Mech. Engrg.*, vol. 197, pp. 2119-2130.

Ramšak, M., Škerget, L., Hriberšek, M. & Žunič, Z., 2005. A multidomain boundary element method for unsteady laminar flow using stream function-vorticity equations. *Eng. Anal. Bound. Elem.*, vol. 29, pp. 1-14.

Šarler, B. & Kuhn, G., 1999. Primitive variable dual reciprocity boundary element method solution of incompressible Navier–Stokes equations. *Engineering Analysis with Boundary Elements*, vol. 23, pp. 443-455.

Sheu, T. W. H. & Lin, R. K., 2004. Newton linearization of the incompressible Navier-Stokes equations. *International Journal of Numerical Methods in Fluids*, vol. 44, pp. 297-312.

Tetzlaff, D. M. & Harbaugh, J. W., 1989. Simulating Clastic Sedimentation. *Comput. Meth. Geosciences*. Van Nostrand Reinhold, New York.